İSTANBUL UNIVERSITY CERRAHPAŞA

ORIGINAL ARTICLE
Electrica 2024; 24(3): 627-639

Classifying Two Primary Bearing Defect Causes Via the Highest-Energy Node in Wavelet Packet Decomposition

Meriem Behim, Leila Merabet, Salah Saad

Laboratoire des Systèmes Electromécaniques, Badji Mokhtar University, Annaba, Algeria

Cite this article as: M. Behim, L. Merabet and S. Saad, "Classifying two primary bearing defect causes via the highest-energy node in wavelet packet decomposition," *Electrica*, 24(3), 627-639, 2024.

ABSTRACT

The current research focuses on the study of two main causes of bearing defects: load unbalance and bearing improper lubrication using Dspace 1104 card for three stator current signals acquisition. This study suggests a straightforward and effective technique for identifying and categorizing two different kinds of defects. It consists of introducing the current space vector (CSV) analysis technique to avoid loss of information between the three stator current signals; the resulting signal is then processed by wavelet packet decomposition (WPD) to calculate the energy of the final level WPD nodes. The node containing the highest energy values will be selected to train the Multilayer Perceptron Neural Network (MLP-NN) classifier implemented by round-robin cross-validation technique. The results confirm the efficiency of the proposed procedure in bearing causes defects classification with an average accuracy of 100% for the tests and 99.88% for the training.

Index Terms—Current space vector (CSV) analysis, energy, improper lubrication, load unbalance, multilayer perceptron neural network (MLP-NN), Wavelet packet decomposition (WPD)

I. INTRODUCTION

The induction motor is an important equipment widely used in the industrial world due to its maintainability, ease of use, and its high efficiency. But this machine is faced with electrical and mechanical failures causing its shutdown and this subsequently leads to a loss of productivity in terms of time and cost. It is for this reason and for decades, numerous studies concentrate on the diagnosis of various induction motor malfunctions using several diagnosis techniques such as current monitoring [1–3], acoustic emission [4–6], thermal [7], and vibration techniques [8, 9].

While the rolling bearings represent the most crucial elements in the induction motor so that many investigations are focused on the fault diagnosis of these components, dealing with outer race breakage, inner race, cage and ball breakage as the authors of [10] presented an unsupervised fault diagnosis method for bearing faults diagnosis integrating short-time Fourier transform (STFT) with categorical generative adversarial networks (CatGAN); Ying Zhang et al. [11] also proposed an enhanced convolution neural network (CNN) model using time–frequency images as inputs for bearing fault diagnosis to obtain better training results; While in [12] a multiple wavelet regularized deep residual network (MWR-DRN) has been developed by a set of auxiliary wavelet basis functions (WBFs) to increase the diversity of deep neural network input and prevent it from over fitting even with a small training set; Wang et al. [13] have used a Time-frequency symmetry dot pattern transformation technique to get two dimension representation, and a multi-scale transfusion network to diagnose bearing defect through vibration signals; the authors of [14] developed an on-rotor sensing system for wireless vibration measurement instead of traditional on-house sensing accelerometer to diagnose rolling bearing fault.

There are numerous internal and external issues that can lead to bearing breakage such as improper selection or design of bearings; improper material selection and quality; incorrect assembly, use, and maintenance; overload and poor lubrication [15, 16]. Therefore it would be better to diagnose and treat these causes to prevent bearing damages; some works are conducted in this field where the authors of [17] have introduced the current space vector combined

Corresponding author:
Meriem Behim

E-mail:
meriembehim96@gmail.com

Received: March 27, 2024

Revision requested: May 4, 2024

Last revision received: July 9, 2024

Accepted: August 1, 2024

Publication Date: October 1, 2024

DOI: 10.5152/electrica.2024.24029

with Wavelet Packet Decomposition (WPD) technique to diagnose load unbalance defect switch energy level variations, where a simple tool has been proposed by [18] analyzing the ranges values of the discrete wavelet transform to diagnose bearing improper lubrication defect. He et al. [19] provided an overview of frequent electrical bearing failure types in mechanical systems, covering different damages and lubrication failures; the problem of the influence of bearing installation faults on lubrication and bearing wear defects is solved in paper [20] using a finite difference approach and super-relaxation iteration method.

With the use of Dspace card for the acquisition of three stator current signals and current space vector (CSV) technique to prevent information loss, the present work aims to address two primary causes of bearing faults: load unbalance and improper lubrication, which have not been widely considered when the current signals are concerned. Additionally, the highest energy level of WPD is selected in order to train the MLP-NN classifier to diagnose the defects. To ensure the effectiveness of the neural network in defect classification, a round-robin cross-validation technique was employed. The findings demonstrate the efficiency of the proposed approach in classifying bearing defects, based on the selection of the highest energy nodes, achieving an average accuracy of 100% in testing and 99.88% in training.

II. THEORETICAL BACKGROUND

A. Bearing Defects

Rolling bearings are among the primary parts of induction motors (IMs) which consist of rolling elements, cages, and outer and inner rings.

As the WPD is used in this work, it is important to recall the well known equations of vibration frequencies caused by bearing failures [21]:

$$\begin{cases} f_{OR}(Hz)=\dfrac{Z}{2}f_r\left(1-\dfrac{B_D}{C_D}cos\beta\right) \\ f_{IR}(Hz)=\dfrac{Z}{2}f_r\left(1+\dfrac{B_D}{C_D}cos\beta\right) \\ f_B(Hz)=f_r\dfrac{C_D}{2B_D}\left[1-\left(\dfrac{B_D}{C_D}cos\beta\right)^2\right] \\ f_C(Hz)=\dfrac{f_r}{2}\left(1-\dfrac{B_D}{C_D}cos\beta\right) \end{cases} \quad (1)$$

where: f_{OR}: outer race fault, f_{IR}: inner race fault, f_B: ball fault, f_C: cage fault, Z: number of rollers/balls, B_D: ball diameter, C_D: pitch circle diameter of bearing, β: the contact angle in radians, and f_r is the rotational frequency.

The variation of stator current is a result of these mechanical vibrations creating anomalies in the air gap flux density [21]. These frequencies are computed as:

$$f_b=\left|f_e\pm kf_v\right| \quad (2)$$

where: k = 1, 2, . . ., f_b is the bearing defect frequency, f_v represents one of the vibration characteristic frequencies calculated by (1), and f_e represents the supply frequency.

Owing to several factors, bearings are progressively deteriorated as investigated in the literature [22–24], and the main causes of bearing defects are resumed as follows:

a. Lubrication failure: related to insufficiency, degradation or improper lubrication which can lead to bearing overheating.
b. Corrosion and contamination: caused by the insertion of foreign particles into lubricant or deteriorated corrosive solution.
c. Excessive load which means application of load excessively.
d. Incorrect assembly and misalignment: the interference fit mechanism should be used for mounting bearings on rotating rings and the lock nuts must be tight.
e. Load unbalance defect:

As illustrated in Fig. 1, the irregular mass distribution along a rotational axis represents the load unbalance fault. This mass experiences a centrifugal force, which causes torque oscillations at specific frequencies that are frequently connected to the mechanical speed of the motor. As a result, peaks in the current spectrum are produced at certain frequencies that may be represented using the following formula [17].

$$f_{lu}=f_e\pm kf_r \quad (3)$$

with: f_{lu}: load unbalance frequency, f_e: stator supply frequency, f_r: rotation frequency, and k = 1, 2, 3 ….

B. Current Space Vector

The Current Space Vector (CSV) technique relies on the concepts of symmetrical components introduced by Charles Fortescue in 1918. This technique is used to analyze and control three-phase electrical systems by decomposing an unbalanced system into several balanced systems [25, 26].

Fortescue's concept involves decomposing a polyphase unbalanced system into several balanced systems, known as symmetrical components. For a three-phase system, this results in three components:

*Positive Sequence Component (i_p):

- The three vectors (phasors) have the same magnitude.
- They are spaced 120 degrees apart from each other.
- The phase sequence is the same as the original system I_{abc}.

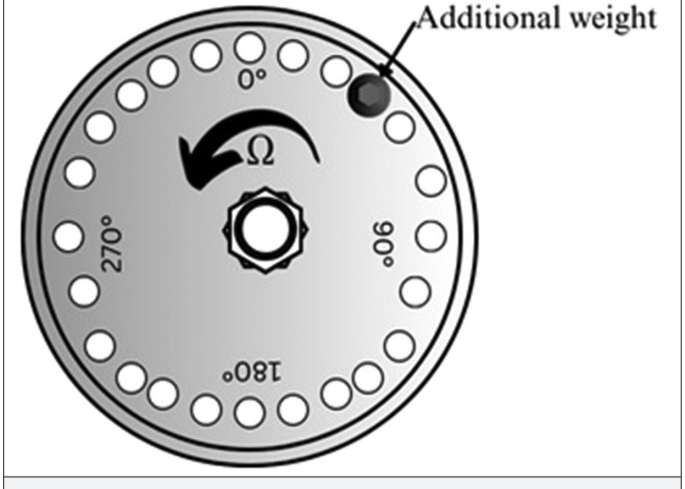

Fig. 1. Load unbalance.

$$i_p = \frac{1}{3}\left(I_a + aI_b + a^2 I_c\right) \quad (4)$$

*Negative Sequence Component (i_n):

- The three vectors have the same magnitude.
- They are also spaced 120 degrees apart from each other.
- The phase sequence is opposite to that of the original system.

$$i_n = \frac{1}{3}\left(I_a + a^2 I_b + aI_c\right) \quad (5)$$

*Zero Sequence Component (i_0):

- The three vectors have the same magnitude.
- They are in phase with each other (no phase difference).

$$i_0 = \frac{1}{6}\left(I_a + I_b + I_c\right) \quad (6)$$

The decomposition of the three-phase stator currents into these three components can be represented by a matrix. Generally, this transformation uses Clarke and Park transformations to move from phase coordinates to symmetrical component coordinates and vice versa.

$$\begin{bmatrix} i_p(t) \\ i_n(t) \\ i_0(t) \end{bmatrix} = \frac{1}{3}\begin{bmatrix} 1 & a & a^2 \\ 1 & a^2 & a \\ \frac{1}{2} & \frac{1}{2} & \frac{1}{2} \end{bmatrix}\begin{bmatrix} i_{as}(t) \\ i_{bs}(t) \\ i_{cs}(t) \end{bmatrix} \quad (7)$$

This matrix represents the transformation that allows moving from phase components to symmetrical components (zero, positive, and negative sequence).

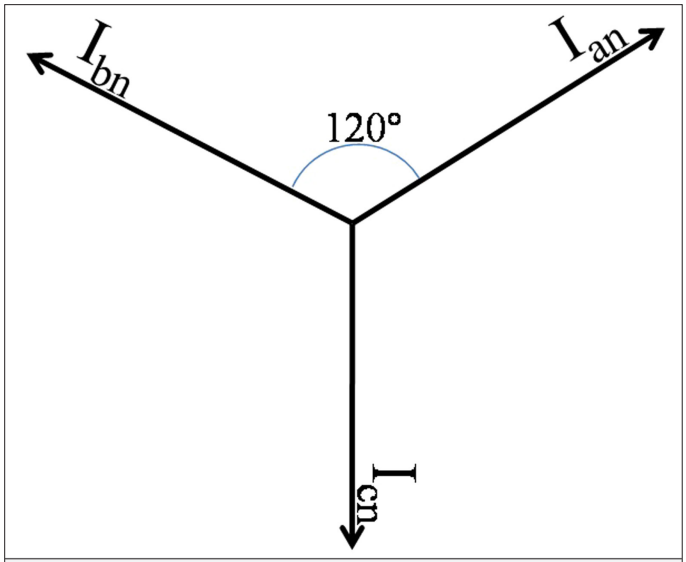

Fig. 3. Current negative sequence components.

In the Current Space Vector technique, these symmetrical components allow for better analysis of currents in a motor or other three-phase device. By using the symmetrical components decomposition, it is possible to:

- Identify and isolate imbalances and harmonics in the system.
- Improve modulation and control of currents in inverters.
- Optimize motor performance in real time by adjusting controls to compensate for imbalances and distortions.

The mentioned figures (Figs. 2–4) visually illustrate these components:

Figure 2 (Positive Sequence Component), shows three phasors of the same magnitude, spaced 120 degrees apart, in the same sequence as the original system.

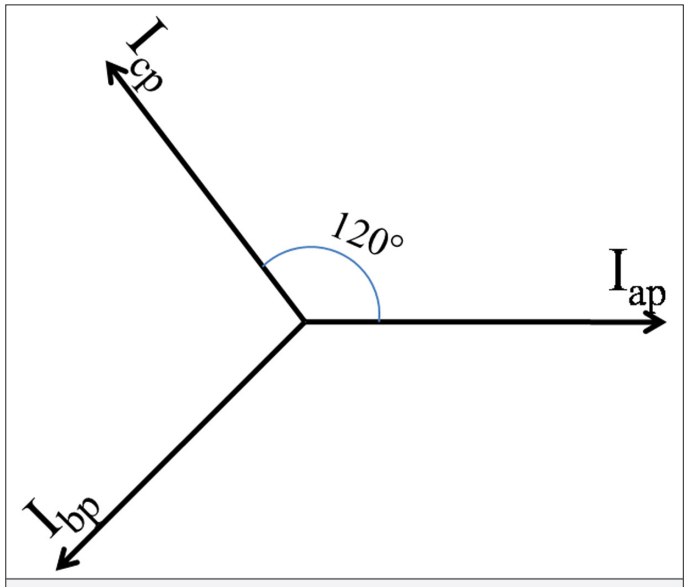

Fig. 2. Current positive sequence components.

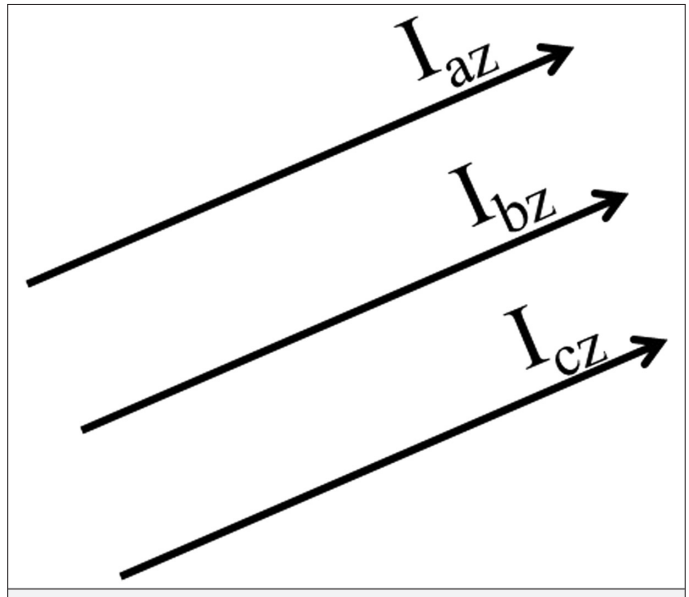

Fig. 4. Current zero sequence components.

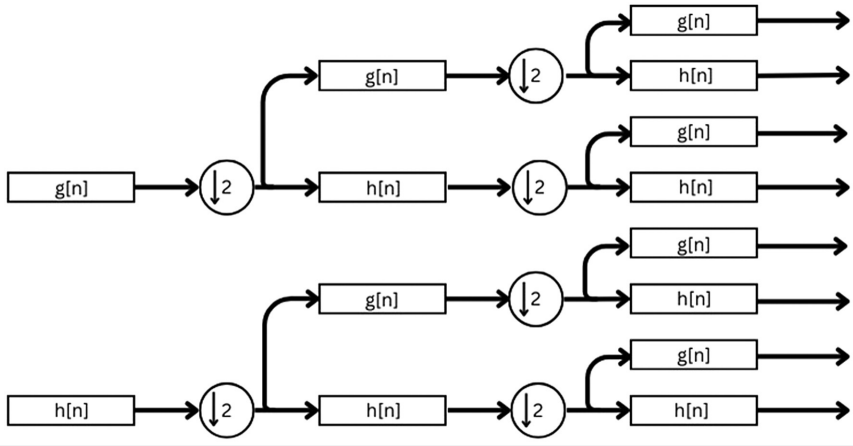

Fig. 5. WPD tree.

Figure 3 (Negative Sequence Component), shows three phasors of the same magnitude, spaced 120 degrees apart, but in an opposite sequence.

Figure 4 (Zero Sequence Component) shows three phasors of the same magnitude, with no phase difference between them.

The system will only consider the positive sequence if it is balanced, which means [27]:

$$i(t)=\frac{1}{3}\left[i_{as}(t)+ai_{bs}(t)+a^2i_{cs}(t)\right] \tag{8}$$

where: $a=e^{-j2/3\pi}$ is the Fortescue operator.

In summary, the Current Space Vector method allows for a detailed analysis and optimized control of three-phase systems, leveraging the concepts of symmetrical components to better understand and regulate currents in these systems.

C. Energy of Wavelet Packet Decomposition

The WPD generates, without data loss or redundancy, an approximation coefficient holding low-frequency information and a detail coefficient storing high-frequency information of the original signal at each level using a low-pass filter *h[k]* and a high-pass filter *g[k]*, respectively [28]. Decomposed signals calculated at different decomposition levels can be calculated as:

$$\begin{cases} W_{i,2j}(n)=\sum_k h[k]W_{i-1,j}(2n-k) \\ W_{i,2j+1}(n)=\sum_k g[k]W_{i-1,j}(2n-k) \end{cases} \tag{9}$$

The procedure yields the tree structures seen in Fig. 5 and can be performed on several levels [29, 30].

The energy represents a strong indicator for fault classification that serves the purpose of quantifying the energy content of various frequency bands or time intervals in order to capture significant signal features that are relevant for classification.

The energy eigenvalue of each frequency band at a decomposition level *j* is found as follows [31]:

$$E_j=\sum_{n=1}^{N}\left|X_j(n)\right|^2 \tag{10}$$

where: $X_j(n)$ are the wavelet packet coefficients.

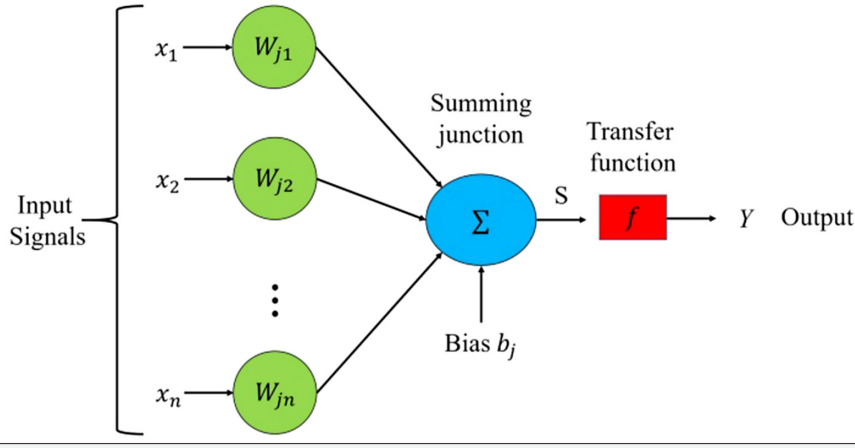

Fig. 6. Model of an artificial neuron.

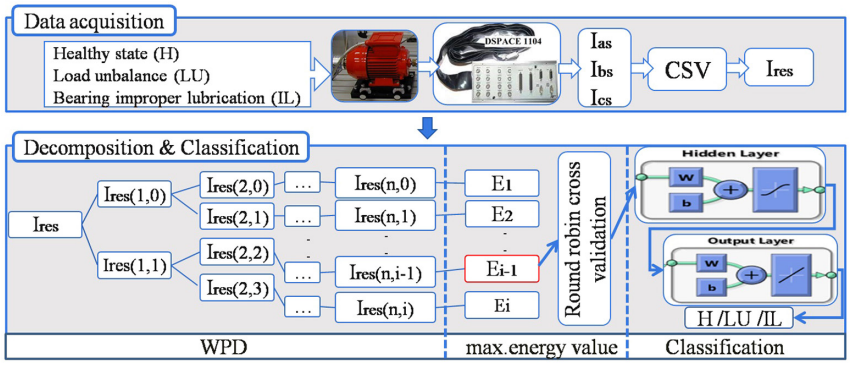

Fig. 7. The flow chart of the proposed methodology.

D. MLP-NN

MLP-NN is the most popular tool for fault classification due to its ease of use and its resistance to noisy input data, which is useful in fault classification tasks where measurement errors or noise may contaminate the input signals [32].

The most popular applications of MLP-NN are composed of an input layer, one or more hidden layers, and an output layer. Each layer's output data represents entries for the layer that comes after it, where, these data are weighted by weights (w_{jn}) subject to error learning, following rules and algorithms [33]. This whole procedure is illustrated by equation (8) and the diagram presented in Fig. 6.

$$Y = f\left(\sum_{i=1}^{n} W_{ji} x_i + b_j\right) \tag{11}$$

where: x_n: input data, W_{jn}: weights, b_j: bias, Y: output and f: transfer function.

III. PROPOSED METHODOLOGY

The proposed methodology (Fig. 7) of this work consists of five steps:

Step 1: Data acquisition using Dspace 1104;

Step 2: Compute the CSV of the three-phase current signals (Ias: statoric current phase A, Ibs: statoric current phase B, Ics: statoric current phase C);

Step 3: Decomposition of the obtained CSV signals by WPD using Daubechies mother wavelet (db44) which is renowned for its orthogonality and high localization properties in both the time and frequency domains, which makes them useful in signal processing analysis and reconstruction processes [28];

Step 4: Calculation of energy for the WPD coefficients;

Step 5: Defects classification using MLP-NN enhanced by round robin technique, by giving as inputs the highest energy level of the WPD coefficients.

IV. EXPERIMENTAL SETUP FOR DATA ACQUISITION

The designed experimental setup (Fig. 8) consists of one pole pair induction machine with an encoder, a PC, connectors, three current sensors coupled to a Dspace 1104 acquisition card, elastic claw coupling, bearing unit, and balanced flywheel (load). The current signal used in this application was collected at a sampling frequency of 5 KHz, for a rotation speed of 3000 rpm, under different operating conditions: healthy state, improper lubrication of ball bearing element and load unbalance of 10 g as shown in Figs. 8 and 9. Table 1 shows the parameters of the bearing geometry.

V. RESULTS AND DISCUSSIONS

The following computer programs and results are provided using Matlab 2016.b.

Stage 1: Data acquisition

Figure 10 represents the three phases of stator current of the several states: healthy motor, bearing defect and load unbalance. These signals were recorded as explained in the experimental setup. Where the database is composed of 90 signals (90 samples): 30 signals of healthy states, 30 signals of bearing improper lubrication defect and 30 signals of load unbalance defect.

In order to prevent loss of information between the three phases (Ias, Ibs, and Ics), the CSV analysis method was applied to the stator current signal phases using the formula (5). The resultant signal will be used in stage 2 to be decomposed by the WPD.

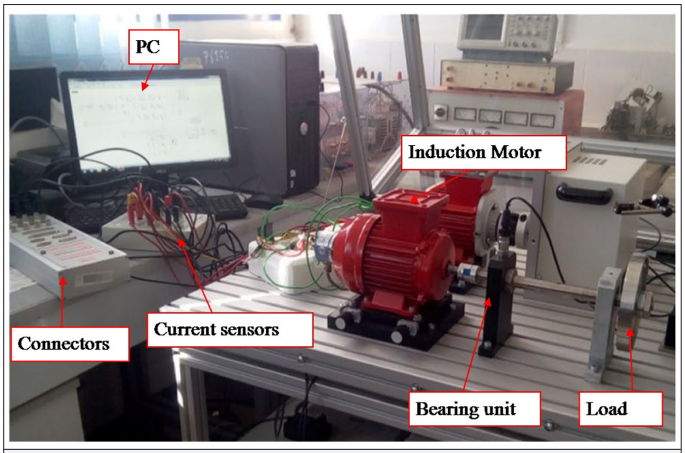

Fig. 8. Experimental setup.

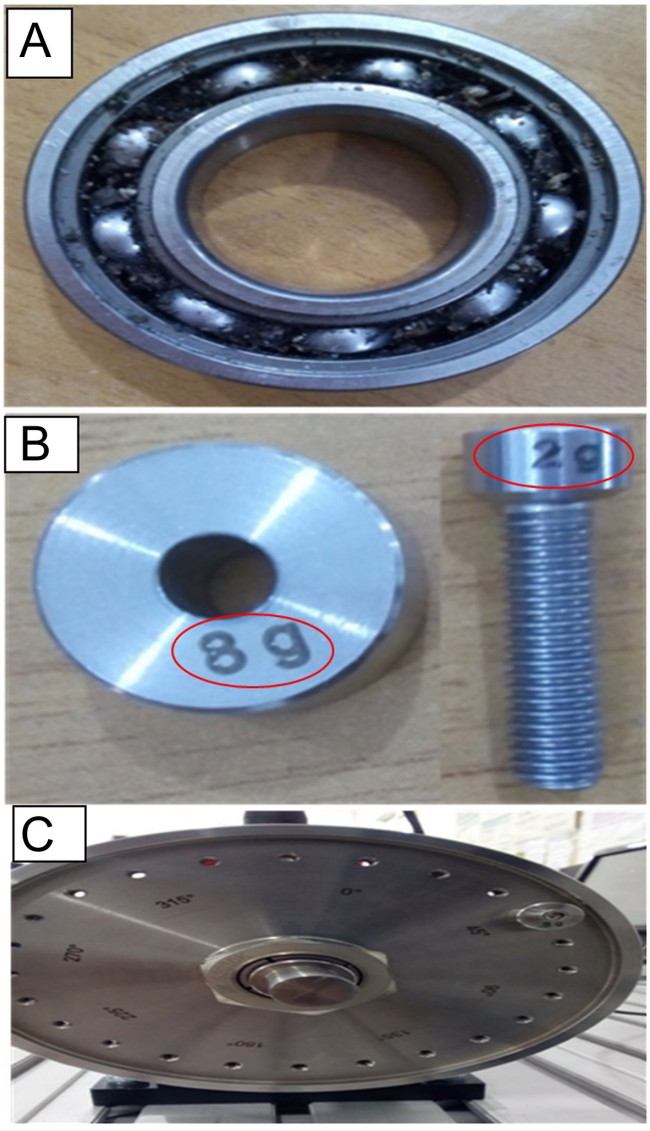

Fig. 9. Adressed faults: a) improper lubrication bearing defect, b) load of 10g, c) load wheel.

Stage 2: Signal decomposition and energy calculation

The WPD of the CSV signal is performed using Daubechies' 'b44' mother wavelet, and the decomposition level is computed as follows [34]:

$$N=\text{int}\left(\frac{\log\left(f_s/f_e\right)}{\log(2)}\right)+2 \quad (12)$$

TABLE I. BEARING PARAMETERS (MM): BALL BEARING 6004-2RSH SKF

Inside Diameter	Outside Diameter	Thickness	Ball Diameter	Pitch Diameter
20	42	12	6	31

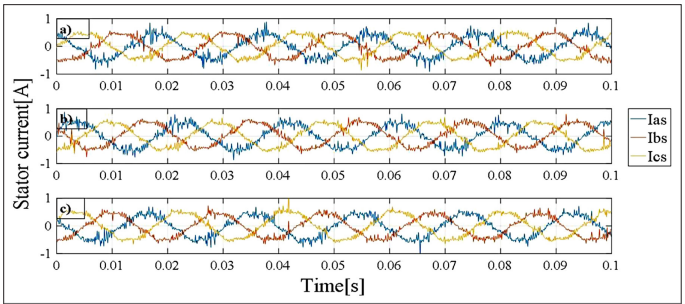

Fig. 10. Stator current signals, a) healthy state, b) improper lubrication defect, c) load unbalance defect.

with: f_s: sampling frequency (f_s = 5 kHz), f_e: supply frequency (f_e = 52 Hz), and so N = 8.

The energy values associated with the eighth-level WPD nodes are shown in Fig. 11. These findings make it clear that the node (8.3) has the energy concentration. So, the energies corresponding to this node will be introduced as inputs to train the MLP-NN.

Stage 3: Fault classification

With the parameters gathered in Table 2, MLP-NN performs the defect classification.

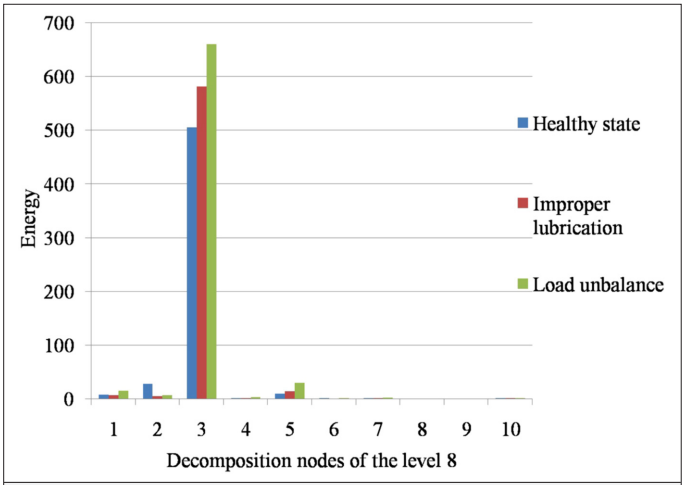

Fig. 11. Energy values at eight level nodes.

TABLE II. MLP-NN DESIGN PARAMETERS

Learning Type	Supervised
Activation function Hidden layer Output layer	 Tansigmoid Purlin
Performance	MSE
Weights initialization	Random
Stopped criteria Minimum gradient Max.Epochs Mu	 10^{-7} 1000 0.001

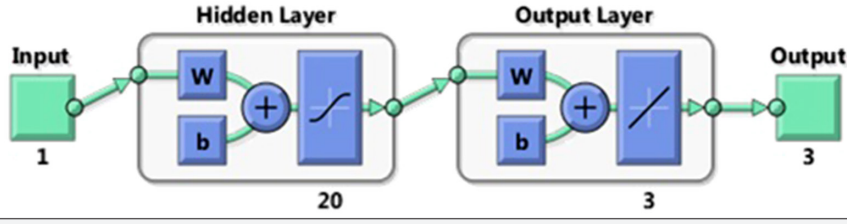

Fig. 12. MLP-NN architecture.

In order to ensure the performance of the MLP-NN, a round-robin cross-validation algorithm was applied. This technique is based on the decomposition of the dataset into *k* equal-sized parts. *(k–1)* parts were used for the training of the MLP-NN and one remaining part for the test [35]. The same process will be held on all the parts, this ensures that each part is represented adequately in both the training and testing phases [36].

In our case, the dataset is divided into 10 equal parts.

For each class, 9 out of 10 parts are used for training, and the remaining 1 part is used for testing.

The process is repeated in a round-robin manner, meaning that each class takes turns being the focus of training and testing.

A confusion matrix is generated to summarize the results. The rows of the table represent the true class labels, while the columns represent the assigned class labels predicted by the model. Each cell in the table contains the estimated value for the number of samples falling into that category.

Additionally, the standard deviation of each entry in the contingency table is calculated. Since the estimates in the contingency table follow a multinomial distribution, the standard deviation can be easily computed.

Figure 12 illustrates the MLP-NN classifier implemented using Matlab. This classifier consists of:

Input layer: contains one input corresponding to a vector of energy.

Hidden layer: comprises 20 neurons, determined through extensive performance testing with various neuron counts. This layer uses a hyperbolic tangent "Tansigmoid" activation function to center activations around zero, aiding convergence during training and facilitating backpropagation.

Output layer: contains 3 neurons, representing bits that correspond to different classes as detailed in Table 3. This layer employs the "purelin" linear activation function, which outputs its input directly without any non-linear transformation.

TABLE III. DEFECTS CODIFICATION

Condition	Class	Codification
Healthy state	1	100
Improper lubrication	2	010
Load unbalance	3	001

The performance rate is calculated as the ratio of correct classifications to total tests of classification:

$$P\% = \frac{C}{T}100 \tag{13}$$

where: *P*: the performance rate, *C*: the number of correct classification and *T*: the number of total tests.

Figures 13–22 represent the best validation performance, and train and test confusion matrix for the ten rounds. For the mean square error, it is clear that the training is well done when both train, test, and validation do not exceed the value of 1e–4. The MLP-NN performs 100% for all the rounds' tests and trains, except round 5 accuracy achieved only 98.8% due to the misclassification of one sample. However, this misclassification in round 5 does not affect the tests performance.

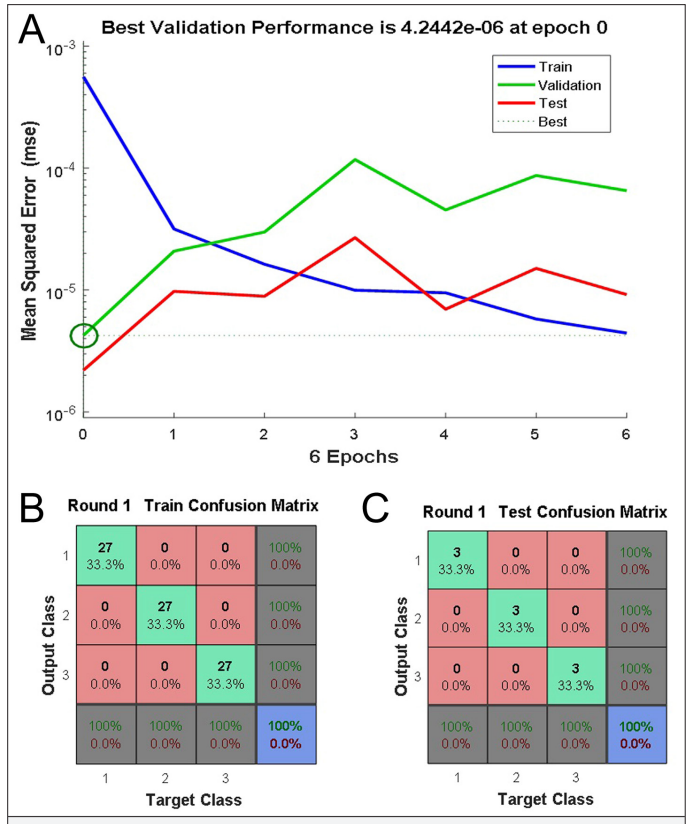

Fig. 13. Round 1: a) Best validation performance, b) Train confusion matrix, c) Test confusion matrix.

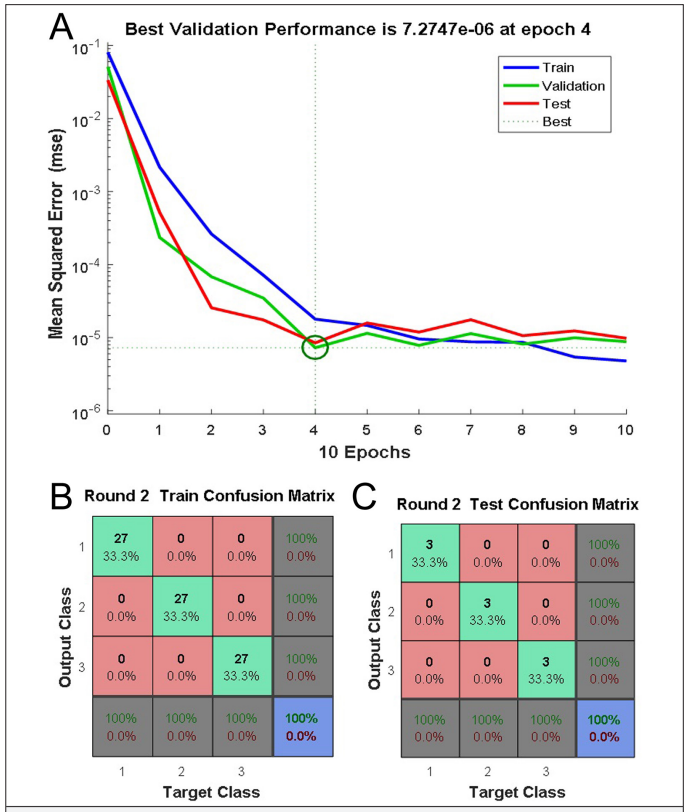

Fig. 14. Round 2: a) Best validation performance, b) Train confusion matrix, c) Test confusion matrix.

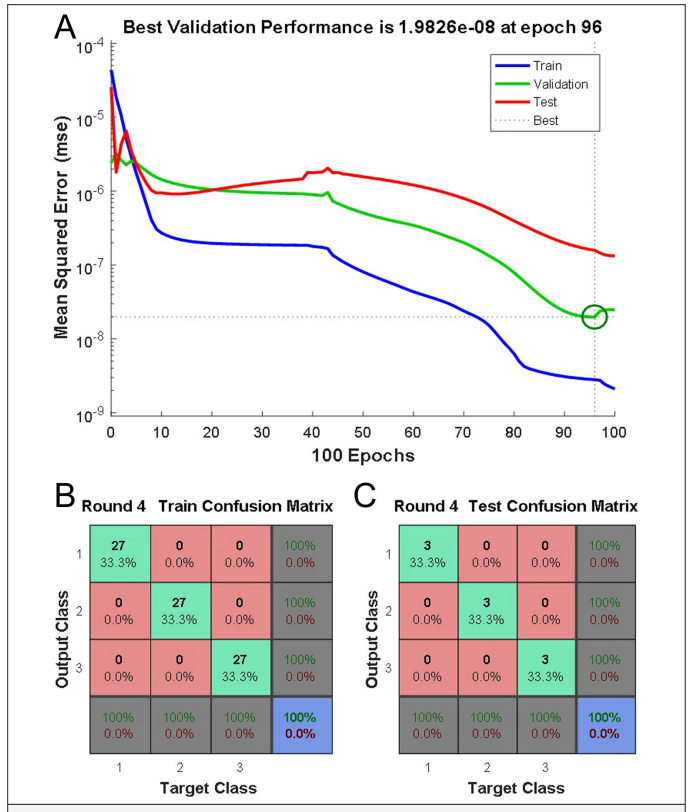

Fig. 16. Round 4: a) Best validation performance, b) Train confusion matrix, c) Test confusion matrix.

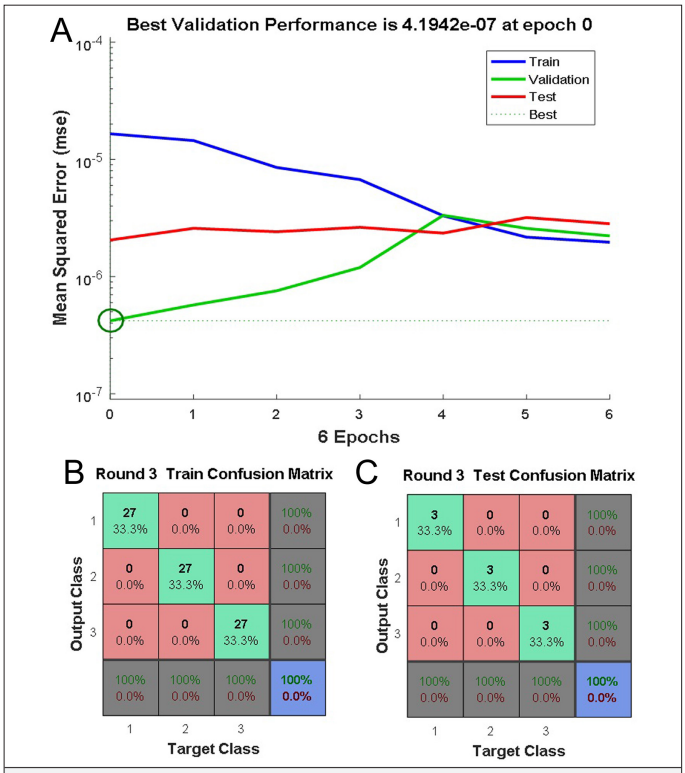

Fig. 15. Round 3: a) Best validation performance, b) Train confusion matrix, c) Test confusion matrix.

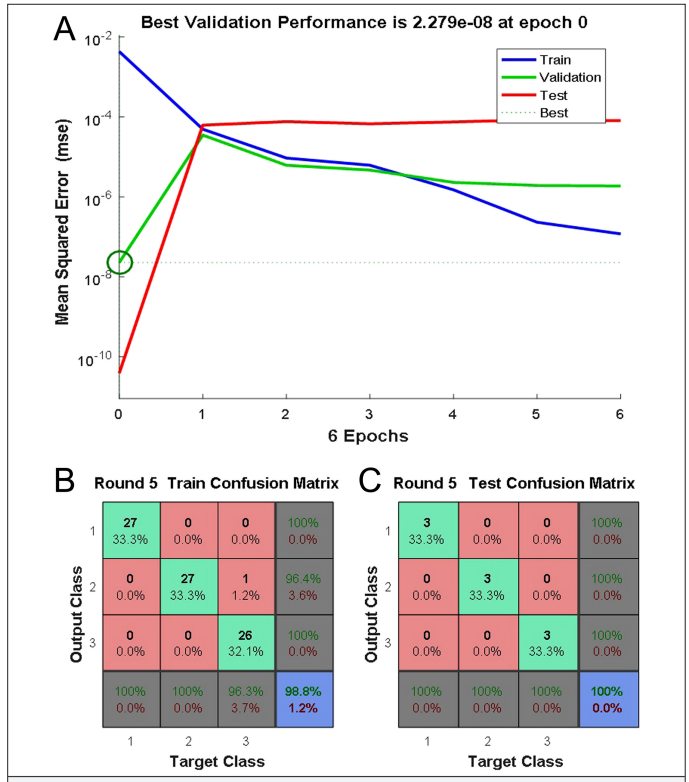

Fig. 17. Round 5: a) Best validation performance, b) Train confusion matrix, c) Test confusion matrix.

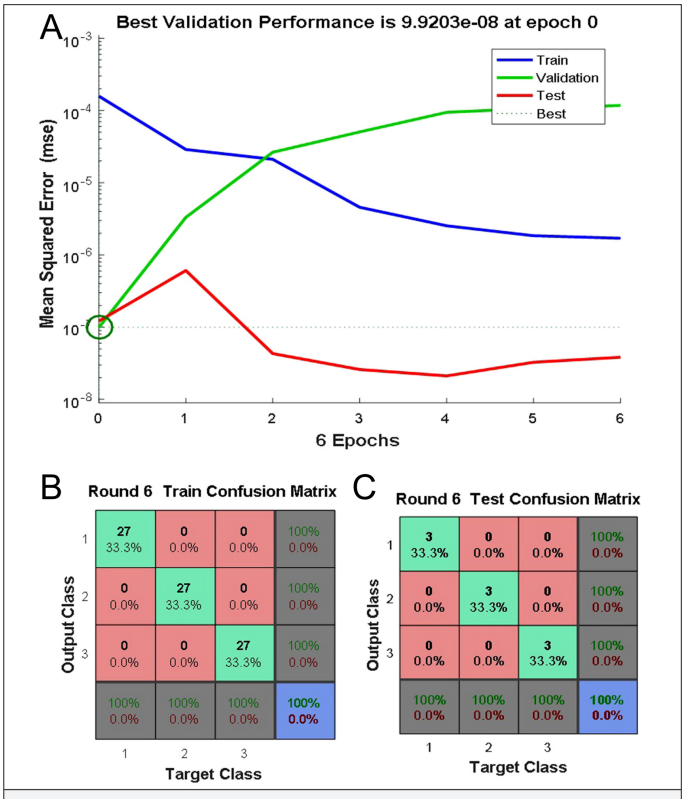

Fig. 18. Round 6: a) Best validation performance, b) Train confusion matrix, c) Test confusion matrix.

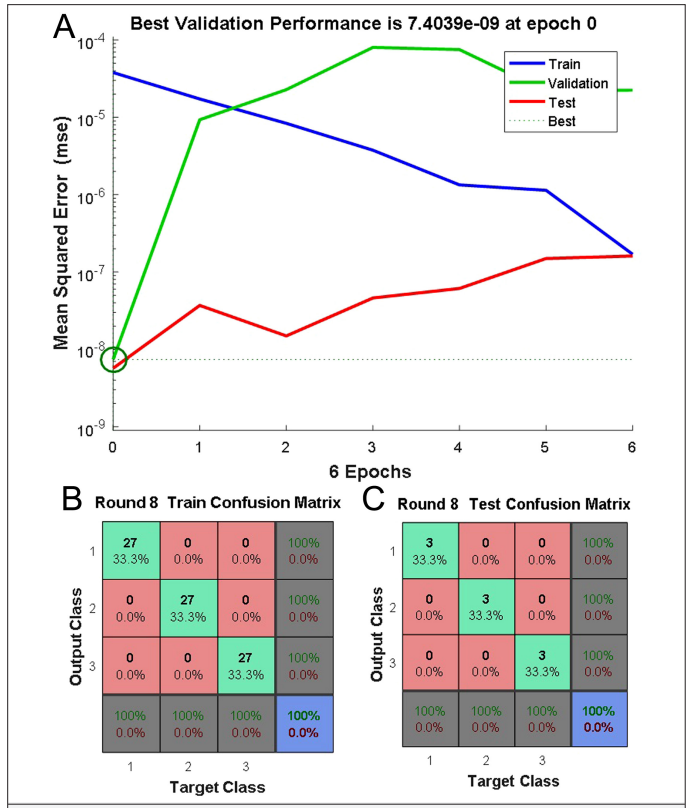

Fig. 20. Round 8: a) Best validation performance, b) Train confusion matrix, c) Test confusion matrix.

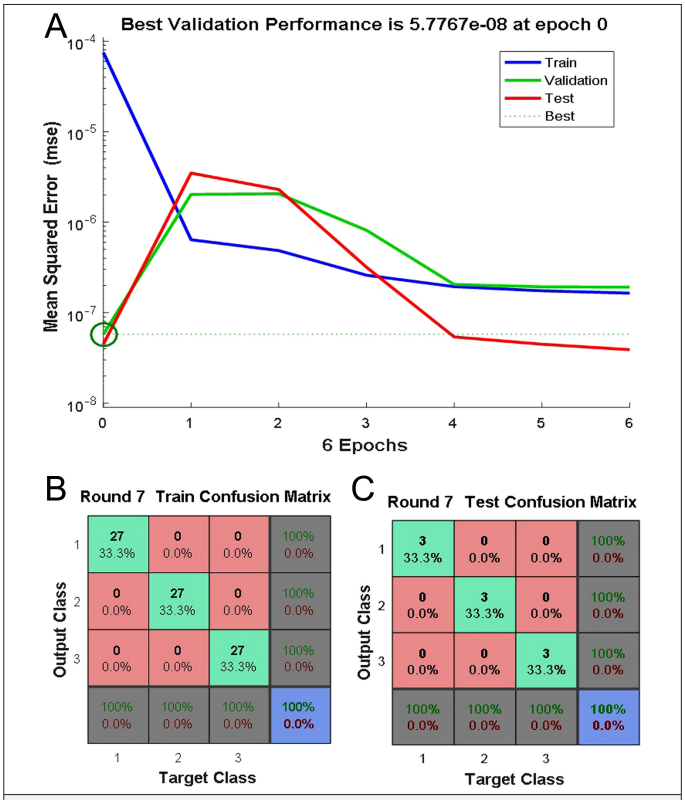

Fig. 19. Round 7: a) Best validation performance, b) Train confusion matrix, c) Test confusion matrix.

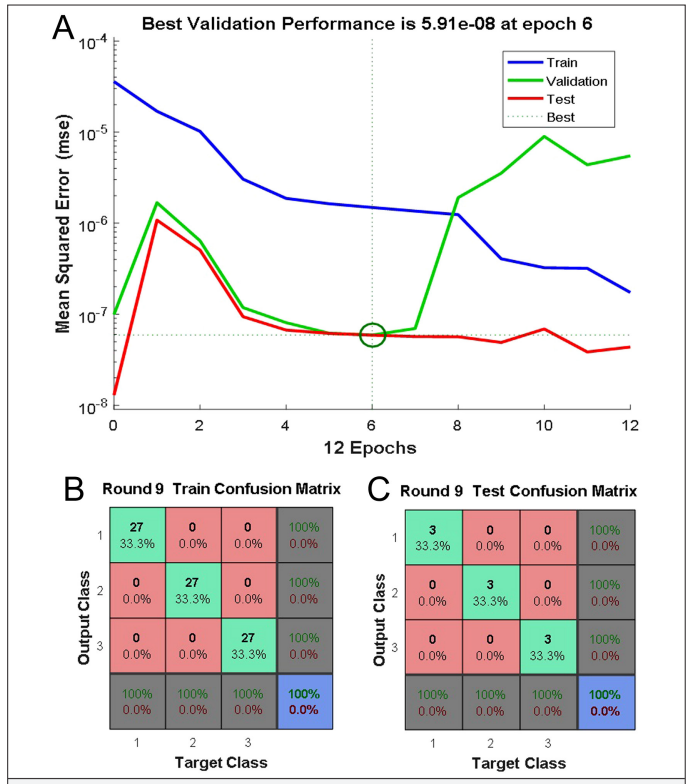

Fig. 21. Round 9: a) Best validation performance, b) Train confusion matrix, c) Test confusion matrix.

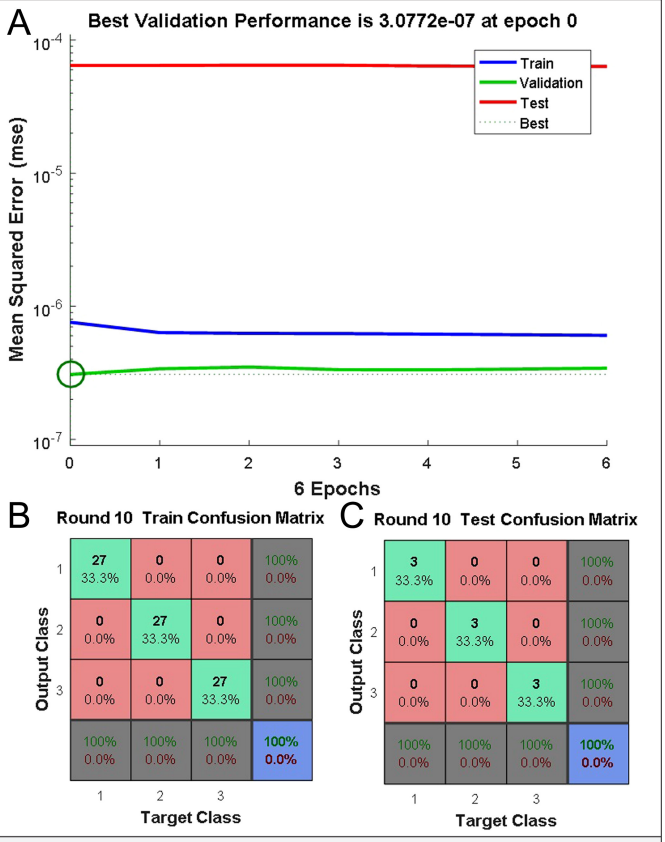

Fig. 22. Round 10: a) Best validation performance, b) Train confusion matrix, c) Test confusion matrix.

Table 4 summarizes the total regression, the training accuracy, and the test accuracy for the ten rounds. When categorizing data based on defect types of three classes, with an average accuracy of 100% for the tests and 99.88% for the training with a high regression superior to 0.999, except for round 5 where the regression is equal to 0.99315; however, this regression does not affect the tests performance. These results confirm the effectiveness of the proposed method for load unbalance and improper lubrication bearing defects classification.

The effectiveness of the classification is then confirmed, providing other quality measures represented by the following metrics [37]:

Sensitivity, also called recall or true positive rate, measures the proportion of true positives correctly identified among truly positive cases.

Specificity measures the proportion of true negatives correctly identified among truly negative cases.

Precision measures the proportion of correct positive predictions among total positive predictions.

F1-Score is the harmonic average of precision and sensitivity. It provides a balance between the two, especially useful when classes are unbalanced.

Matthews Correlation Coefficient (MCC), is a measure that takes into account TP, TN, FP, and FN and gives a balanced assessment

TABLE IV. CLASSIFICATION RESULTS

Round	Total R	Train Acc (%)	Test Acc (%)
1	0.99911	100	100
2	0.99997	100	100
3	0.99997	100	100
4	1	100	100
5	0.99315	98.8	100
6	0.99975	100	100
7	0.99988	100	100
8	0.99994	100	100
9	1	100	100
10	0.99998	100	100
Average	/	99.88	100

of classification performance, even if the classes are of very different sizes. The MCC ranges from −1 to 1, where 1 represents perfect classification, 0 represents random classification, and −1 represents opposite classification.

To calculate the MCC, F1-Score, sensitivity, specificity, and precision metrics, the following formulas of equation (14) were calculated for the different confusion matrices.

$$\begin{cases} Sensitivity = \dfrac{TP}{TP+FN} \\ Specificity = \dfrac{TN}{TN+FP} \\ Precision = \dfrac{TP}{TP+FP} \\ F1-Score = \dfrac{2*Precision*Sensitivity}{Precision+Sensitivity} \\ MCC = \dfrac{(TP*TN)-(FP*FN)}{\sqrt{(TP+FP)(TP+FN)(TN+FP)(TN+FN)}} \end{cases} \quad (14)$$

where:

TP (True Positives): Number of true positives (positive cases correctly identified).

TN (True Negatives): Number of true negatives (negative cases correctly identified).

FP (False Positives): Number of false positives (negative cases incorrectly identified as positive).

FN (False Negatives): Number of false negatives (positive cases incorrectly identified as negative).

Table 5 represents Sensitivity, Specificity, Precision, F1-Score, and MCC mean values for the ten rounds for both train and tests. The metrics' results show that the classification model performs extremely well on the training and test data.

TABLE V. METRICS' RESULTS

	Sensitivity		Specificity		Precision		F1-Score		MCC	
	Train	Test	Train	Test	Train	Test	Train	Test	Train	Test
Round 1	1	1	1	1	1	1	1	1	1	1
Round 2	1	1	1	1	1	1	1	1	1	1
Round 3	1	1	1	1	1	1	1	1	1	1
Round 4	1	1	1	1	1	1	1	1	1	1
Round 5	0.988	1	0.994	1	0.988	1	0.987	1	0.992	1
Round 6	1	1	1	1	1	1	1	1	1	1
Round 7	1	1	1	1	1	1	1	1	1	1
Round 8	1	1	1	1	1	1	1	1	1	1
Round 9	1	1	1	1	1	1	1	1	1	1
Round 10	1	1	1	1	1	1	1	1	1	1

VI. CONCLUSION

In this paper, an online fault diagnostic procedure combining WPD with MLP-NN classifier architecture has been proposed for fault diagnosis for a fixed-speed IM in three operating conditions: healthy state, improper lubrication bearing defect and load unbalance. The procedure is based on using Dspace for currents acquisition and the current support vector (CSV) technique for three-phase stator currents analysis. The resultant current signal is decomposed into different frequency groups by the WPD process, and the energy of each frequency sub-band of the eight-level decomposition was computed, then the highest energy node was selected to train the MLP-NN enhanced by a round-robin technique with 10 rounds. The findings validate the effectiveness of the proposed method in classifying bearing causes defects, achieving an average accuracy of 100% in test scenarios and 99.88% during training, caused by the misclassification of one sample during the fifth round of training. This method can also be extended and employed to identify other kinds of induction motor defects in real-time applications.

Availability of Data and Materials: The data that support the findings of this study are available on request from the corresponding author.

Peer-review: Externally peer-reviewed

Author Contributions: Concept – M.B.; Design – M.B.; Supervision – L.M., S.S.; Analysis and/or Interpretation – M.B.; Literature Search – M.B.; Writing – M.B.; Critical Review – L.M., S.S.

Declaration of Interests: The authors have no conflict of interest to declare.

Funding: The authors declared that this study has received no financial support.

REFERENCES

1. H. Cherif et al., "Early detection and localization of stator inter-turn faults based on discrete wavelet energy ratio and neural networks in induction motor," *Energy*, vol. 212, p. 118684, 2020. [CrossRef]
2. B. Guan, X. Bao, H. Qiu, D. Yang, "Enhancing bearing fault diagnosis using motor current signals: A novel approach combining time shifting and CausalConvNets," *Measurement*, vol. 226, p. 114049, 2024. [CrossRef]
3. T.-T. Vo, M.-K. Liu, M.-Q. Tran, "Harnessing attention mechanisms in a comprehensive deep learning approach for induction motor fault diagnosis using raw electrical signals," *Eng. Appl. Artif. Intell.*, vol. 129, p. 107643, 2024. [CrossRef]
4. A. Glowacz, and Z. Glowacz, "Diagnosis of stator faults of the single-phase induction motor using acoustic signals" *Appl. Acoust.*, vol. 117, pp. 20–27, 2017. [CrossRef]
5. A. Glowacz, W. Glowacz, Z. Glowacz, J. Kozik, "Early fault diagnosis of bearing and stator faults of the single-phase induction motor using acoustic signals," *Measurement*, vol. 113, pp. 1–9, 2018. [CrossRef]
6. A. Choudhary, R. K. Mishra, S. Fatima, B. K. Panigrahi, "Multi-input CNN based vibro-acoustic fusion for accurate fault diagnosis of induction motor," *Eng. Appl. Artif. Intell.*, vol. 120, p. 105872, 2023. [CrossRef]
7. A. Glowacz, "Thermographic fault diagnosis of electrical faults of commutator and induction motors," *Eng. Appl. Artif. Intell.*, vol. 121, p. 105962, 2023. [CrossRef]
8. F. Li, L. Wang, D. Wang, J. Wu, H. Zhao, "An adaptive multiscale fully convolutional network for bearing fault diagnosis under noisy environments," *Measurement*, vol. 216, p. 112993, 2023. [CrossRef]
9. B. Song, Y. Liu, J. Fang, W. Liu, M. Zhong, X. Liu, "An optimized CNN-BiLSTM network for bearing fault diagnosis under multiple working conditions with limited training samples," *Neurocomputing*, vol. 574, p. 127284, 2024. [CrossRef]
10. H. Tao, P. Wang, Y. Chen, V. Stojanovic, H. Yang, "An unsupervised fault diagnosis method for rolling bearing using STFT and generative neural networks," *J. Franklin Inst.*, vol. 357, no. 11, pp. 7286–7307, 2020. [CrossRef]
11. Y. Zhang, K. Xing, R. Bai, D. Sun, Z. Meng, "An enhanced convolutional neural network for bearing fault diagnosis based on time–frequency image," *Measurement*, vol. 157, p. 107667, 2020. [CrossRef]
12. M. Zhao, B. Tang, L. Deng, M. Pecht, "Multiple wavelet regularized deep residual networks for fault diagnosis," *Measurement*, vol. 152, p. 107331, 2020. [CrossRef]
13. Z. Wang, D. Shi, Y. Xu, D. Zhen, F. Gu, A. D. Ball, "Early rolling bearing fault diagnosis in induction motors based on on-rotor sensing vibrations," *Measurement*, vol. 222, p. 113614, 2023. [CrossRef]
14. Z. Wang et al., "Rolling bearing fault diagnosis method using time-frequency information integration and multi-scale TransFusion network," *Knowl. Based Syst.*, vol. 284, p. 111344, 2024. [CrossRef]
15. Z. Li, L. Li, R. Chen, Y. Zhang, Y. Cui, N. Wu, "A novel scheme based on modified hierarchical time-shift multi-scale amplitude-aware permutation entropy for rolling bearing condition assessment and fault recognition," *Measurement*, vol. 224, p. 113907, 2024. [CrossRef]
16. F. Xu et al., "A review of bearing failure Modes, mechanisms and causes," *Eng. Fail. Anal.*, vol. 152, p. 107518, 2023. [CrossRef]
17. N. Lahouasnia, M. F. Rachedi, D. Drici, S. Saad, "Load unbalance detection improvement in three-phase induction machine based on current space vector analysis," *J. Electr. Eng. Technol.*, vol. 15, no. 3, pp. 1205–1216, 2020. [CrossRef]

18. B. Belkacemi, S. Saad, Z. Ghemari, F. Zaamouche, A. Khazzane, "Detection of induction motor improper bearing lubrication by discrete wavelet transforms (DWT) decomposition," *I2M*, vol. 19, no. 5, pp. 347–354, 2020. [CrossRef]
19. F. He, G. Xie, J. Luo, "Electrical bearing failures in electric vehicles," *Friction*, vol. 8, no. 1, pp. 4–28, 2020. [CrossRef]
20. T. Yang, H. Zhu, S. Fan, J. Wu, J. Yuan, and L. Zheng, "Research on Lubrication Characteristics of Ship Stern Bearings Considering Bearing Installation Errors" *Lubricants*, vol. 11, no. 11, p. 478, 2023. [CrossRef]
21. K. C. Deekshit Kompella, M. Venu Gopala Rao, R. Srinivasa Rao, "Bearing fault detection in a 3 phase induction motor using stator current frequency spectral subtraction with various wavelet decomposition techniques," *Ain Shams Eng. J.*, vol. 9, no. 4, pp. 2427–2439, 2018. [CrossRef]
22. C. Malla, and I. Panigrahi, "Review of Condition Monitoring of Rolling Element Bearing Using Vibration Analysis and Other Techniques" *J. Vib. Eng. Technol.*, vol. 7, no. 4, pp. 407–414, 2019. [CrossRef]
23. P. Gangsar, and R. Tiwari, "Signal based condition monitoring techniques for fault detection and diagnosis of induction motors: A state-of-the-art review" *Mech. Syst. Signal Process.*, vol. 144, p. 106908, 2020. [CrossRef]
24. M. Behim, L. Merabet, S. Saad, "Neural network and L-kurtosis for diagnosing rolling element bearing faults," *J. Electr. Eng. Technol.*, vol. 19, no. 4, pp. 2597–2606, 2024. [CrossRef]
25. G. Cablea, P. Granjon, C. Bérenguer, "Method for computing efficient electrical indicators for offshore wind turbine monitoring," *Insight*, vol. 56, no. 8, pp. 443–448, 2014. [CrossRef]
26. S. K, in 5th IEEE Uttar Pradesh Section International Conference on Electrical, Electronics and Computer Engineering (UPCON). Gorakhpur: IEEE Publications, 2018, pp. 1–6. [CrossRef]
27. M. Behim, L. Merabet, S. Saad, "Diagnosis of supply voltage imbalance using WPD energy enhanced by current space vector (CSV)," in *19th International Multi-Conference on Systems, Signals & Devices (SSD)*. Sétif, Algeria: IEEE Publications, 2022, 2022, pp. 242–245. [CrossRef]
28. R. Rouaibia, Y. Djeghader, and L. Moussaoui, "Artificial neural network and discrete wavelet transform for inter-turn short circuit and broken rotor bars faults diagnosis under various operating conditions" *Electr. Eng. Electromech.*, vol. 3, no. 3, pp. 31–37, 2024. [CrossRef]
29. B. Meriem, M. Leila, and S. Salah, "Time - Frequency method and artificial neural network classifier for induction motor drive system defects classification," *Diagnostyka*, vol. 25, no. 1, pp. 1–11, 2024. [CrossRef]
30. M. Behim, L. Merabet, S. Saad, *Detection and Classification of Induction Motor Faults Using DWPD and Artificial Neural Network: Case of Supply Voltage Unbalance and Broken Rotor Bars*, EasyChair Preprint, vol. 7756. Available: https://easychair.org/publications/preprint_download/TrtH. [Accessed: 24 juillet 2022].
31. M. Gan, C. Wang, C. Zhu, "Construction of hierarchical diagnosis network based on deep learning and its application in the fault pattern recognition of rolling element bearings," *Mech. Syst. Signal Process.*, vol. 72–73, pp. 92–104, 2016. [CrossRef]
32. K. Jankowska, and M. Dybkowski, "Experimental Analysis of the Current Sensor Fault Detection Mechanism Based on Neural Networks in the PMSM Drive System" *Electronics*, vol. 12, no. 5, p. 1170, 2023. [CrossRef]
33. W. Qiao, M. Khishe, S. Ravakhah, "Underwater targets classification using local wavelet acoustic pattern and Multi-Layer Perceptron neural network optimized by modified Whale Optimization Algorithm," *Ocean Eng.*, vol. 219, p. 108415, 2021. [CrossRef]
34. Y. Wei, Y. Li, M. Xu, W. Huang, "A review of early fault diagnosis approaches and their applications in rotating machinery," *Entropy (Basel)*, vol. 21, no. 4, p. 409, 2019. [CrossRef]
35. A. S. Tanenbaum, *Modern Operating Systems*, 2nd ed. Peking: China Machine Press, 2002.
36. T. Hastie, R. Tibshirani, J. H. Friedman, *The Elements of Statistical Learning: Data Mining, Inference, and Prediction in Springer series in statistics*, 2nd ed. New York, NY: Springer, 2009.
37. D. Chicco, and G. Jurman, "The advantages of the Matthews correlation coefficient (MCC) over F1 score and accuracy in binary classification evaluation" *BMC Genomics*, vol. 21, no. 1, p. 6, 2020. [CrossRef]

Meriem Behim received her Master degree in Industrial Management and engineering in Maintenance and Reliability of Industrial technologies from École Superieure de Technologies Idustrielles (ESTI), Annaba, Algeria in 2019. She is currently pursuing the Ph.D. degree at the Laboratoire des Systems Eléctromécaniques (LSEM), Badji Mokhtar University, Annaba. Her Research interests include Electrical machines fault diagnosis And Signal processing.

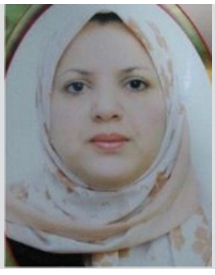

Leila Merabet received Engineer (electrical engineering) and Magister (electrical control) degrees from Annaba University in 1993 and 2001 respectively. She had her Ph.D degree in 2015 and the "Habilitation to supervise research" degree on electrical engineering in 2019. She is working as senior researcher "A". Her research interest includes renewable energy systems, power quality, harmonics, control, PV system, and artificial neuron networks. She authored and co-authored many papers in academic journals, conferences and proceedings.

Salah Saad received Ph.D. degree from Nottingham University UK in 1988. Since 1988 he worked as lecturer, senior lecturer then professor at Badji-Mokhtar Annaba University Algeria. He has conducted many researches projects in power electronics applications, electrical ac and dc drives as well as diagnosis and faults detection in ac machines and vibration sensors. His research interests are mainly in the area of power electronics such as harmonics elimination by active filters, PWM and Space vector modulation control, multilevel inverters and newconverter topologies. He has authored and coauthored many journal and conference papers.